Frontiers in Scientific Research and Technology

Online ISSN: 2682-297
Print ISSN: 2682-2962
http://fsrt.journals.ekb.eg

FSRT J 4 (2022) 7 - 23 10.21608/fsrt.2022.132752.1061

Multi-temporal analysis of Coastal Urbanization and Land Cover Changes in Suez City, Egypt Using Remote Sensing and GIS

Youssef M. Youssef[1,2*], Sugita M[2], Khaled S. Gemail[3], Saada A. Saada[4], Mostafa A. Teama[1], AlBarqawy M.,[5] Abdelaziz El Shinawi[3], Fares Khedr[4]

[1] Department of Science and Mathematical Engineering, Faculty of Petroleum and Mining Engineering, Suez University, Suez 43518, Egypt

[2] Faculty of Life and Environmental Sciences, University of Tsukuba, Tsukuba 305-8572, Japan

[3] Zagazig University, Environmental Geophysics Lab (ZEGL), Department of Geology, Faculty of Science, Zagazig 44519, Egypt

[4] Department of Geology, Faculty of Science, Suez University, Suez 43518, Egypt

[5]Department of Geological and Geophysical Engineering, Faculty of Petroleum and Mining Engineering, Suez University, Suez 43518, Egypt

ARTICLE INFO

Article history:
Received 12 April 2022
Received in revised form 18 April 2022
Accepted 20 April 2022
Available online 21 April 2022

Keywords
Land Use/Land Cover,
Landsat,
Change detection,
Population growth,
Suez

ABSTRACT

Urbanization, which is a global contemporary issue, is rapidly growing in coastal territories with harmful repercussions and unprecedented land cover changes. Therefore, detecting land use/land cover (LULC) change is highly imperative for decision-makers to prepare and implement sustainable developmental projects. The present study attempts to assess coastal urbanization and associated LULC change in Suez city (Egypt) using remote sensing and Geographic Information systems (GIS) techniques. To this end, four multi-temporal Landsat (TM, ETM, and OLI) images acquired in 1986, 2000, 2013, and 2018 were processed and classified. The constructed LULC maps were deemed to be accurate with overall accuracies of over 92%. The change detection results indicate that the urban and vegetation areas were significantly expanded at the expense of dry soil due to rapid development projects over 32 years (1986-2018). The urban area increased dramatically from 28.04 to 52.06 Km2 by more than 80%, while dry bare soil declined by 47.33% over the study period 1986-2018. The vegetation area expanded by 14.52% during 1986-2000 and continued to increase by 25.15% until 2013, then declined by 4.08% in 2018. Results have also shown that most of the fading vegetation areas were mostly transformed into urban areas over the last 32 years. Finally, the urban expansion was strongly governed by population growth, while the natural physiographic conditions constrained the shape of the city. The findings of this work can provide the urban planners with valuable information on LULC changes for more rational planning.

1. Introduction

Coastal regions represent magnificent lands for urbanization because of their distinct locations between inland and sea for logistical, recreational activities, and cultural exchanges. Simultaneously, the population growth is becoming so quick, especially in developing countries (e.g., the Middle East and North Africa, MENA), leading to high population density in coastal cities than in hinterlands (Balk et al., 2009; Engelhardt et al., 2018).

This anthropic pressure has significantly increased in the recent decades, causing fast and unprecedented changes in the land use/land cover (LULC), and therefore, disturbing the physiographic, geological, and hydrological environment (Abd El-Kawy et al., 2011; McMichael et al., 2020; Liaqat et al., 2021; Abu Salem et al., 2021). Consequently, detecting the coastal land use and associated land cover changes, particularly in developing cities, is extremely imperative to meet the United Nations Sustainable Development Goals by 2030.

Monitoring of LULC changes is extremely difficult by traditional methods (i.e., field surveys and archived maps), which limits the scientific understanding of the reasons, driving forces, and consequences of these changes. In this context, geospatial analysis using multi-temporal remotely sensed datasets can objectively provide precise maps describing changes in LULC due to natural and human

* Corresponding authors at Suez University

E-mail addresses: youssef.ibrahim@pme.suezuni.edu.eg (Youssef M. Youssef)

interventions (Singh, 1989; Alberti et al., 2004). Multispectral remote sensing platforms (i.e., ASTER, Landsat, and Sentinel) are the common data sources for detecting the changes in LULC by supplying spatially and temporally continuous data with accurate georeferencing systems. More fundamentally, several change detection methods have been developed to monitor changes in land cover from RS imagery, including spectral indices (Arnous and Green, 2015), unsupervised and supervised classification (Elmahdy and Mohamed, 2016; El-Zeiny et al., 2022), post-classification analysis (Lu et al., 2004; Shalaby and Tateishi, 2007), and image differencing (Moufaddal, 2005). Recently, the integration of remote sensing and Geographic Information System (GIS) techniques has proved to be indispensable in detecting and quantifying land cover changes. Since GIS is conceived to manipulate, store, display, and analyze large and different types of datasets with less expenditure and effort (Karlsson et al., 2017).

The most populous developing country in the MENA area is Egypt (Fig. 1a), with an estimated population of 100 million in 2018 and is expected to rise in the coming decades (UNDESA/PD, 2019). Egypt possessed 36 fast-growing coastal cities, excluding all towns on lakes (Hegazy, 2021). Coastal urbanization not only enhanced socio-economic development in Egypt but also significantly exploited the coastal resources followed by a severe deterioration (Elagouz et al., 2020; El-Zeiny et al., 2022). One of the most important Egyptian coastal cities is Suez due to its outstanding location. This shows through its strategic site at the southern terminus of the Suez Canal, making it a vital trade centre for commodities globally (Fig. 1b). Suez, therefore, has been witnessing rapid urban development since the 1980s that affected the environmental, ecological, and climatological conditions (El Omla and Aboulela, 2012; El-Zeiny et al., 2017; Ahmed, 2018; Youssef et al., 2020; Youssef et al., 2021). Urban planners are in constant need of past and current information on these changes for appropriate land use planning. However, there is a lack of knowledge about the trend and rate of LULC changes that have occurred in Suez over the last years. To this end, the specific aims of this study are the following: to integrate the remotely sensed imagery and field observations along with population census data in the GIS environment (1) to detect the possible influence of coastal urbanization on the LULC changes of the years 1986, 2000, 2013, and 2018 in Suez city, (2) to measure the trend, rate and magnitude of changes between these dates, and finally (3) to inspect the driving forces and factors that dominate the pattern of urban expansion.

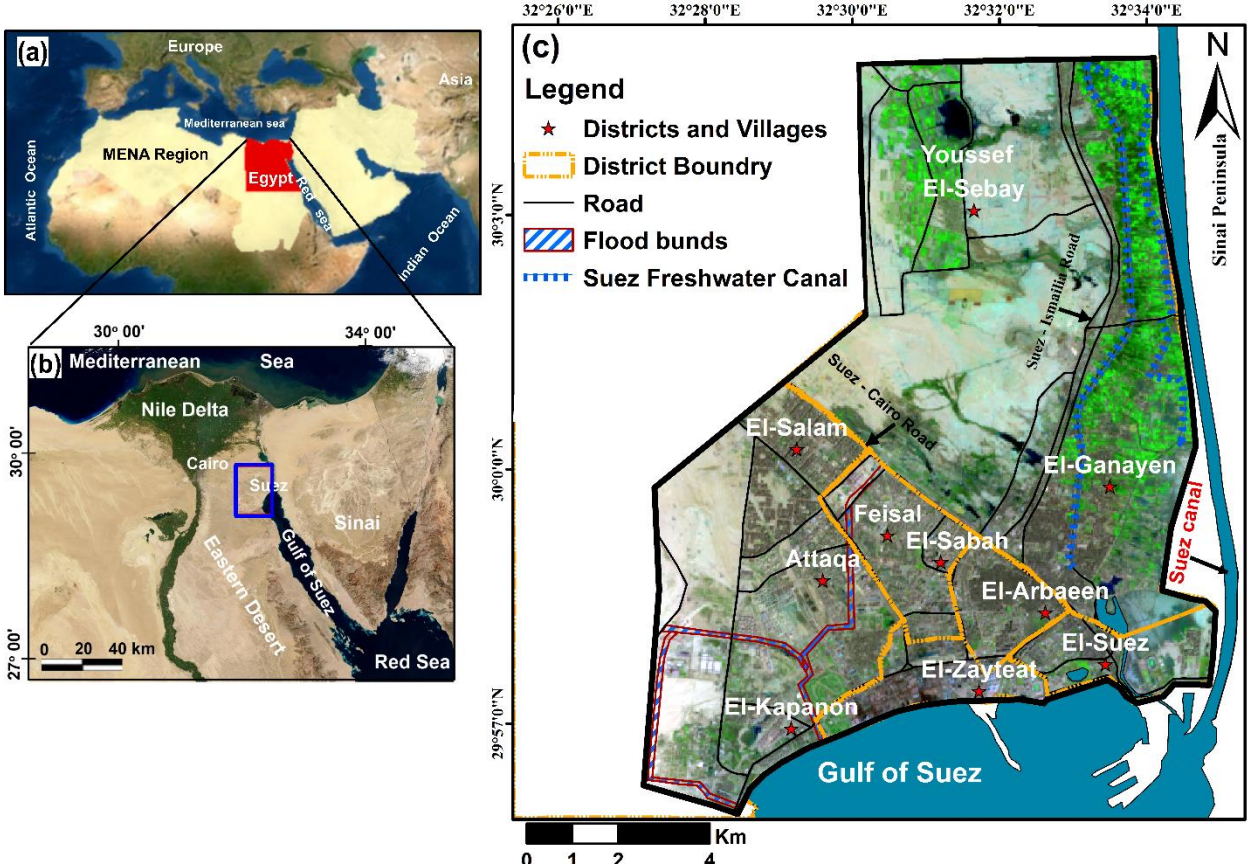

Fig. 1. Location map of the study area: (**a**) Satellite image showing Egypt (red polygon) country located in the middle of the Middle East and North Africa (MENA) region (yellow polygon), (**b**) location map of the study area (blue polygon) in northeastern Egypt, and (**c**) Suez (Landsat-8 (RGB; 753)) with the main infrastructures and districts distribution shown by red stars.

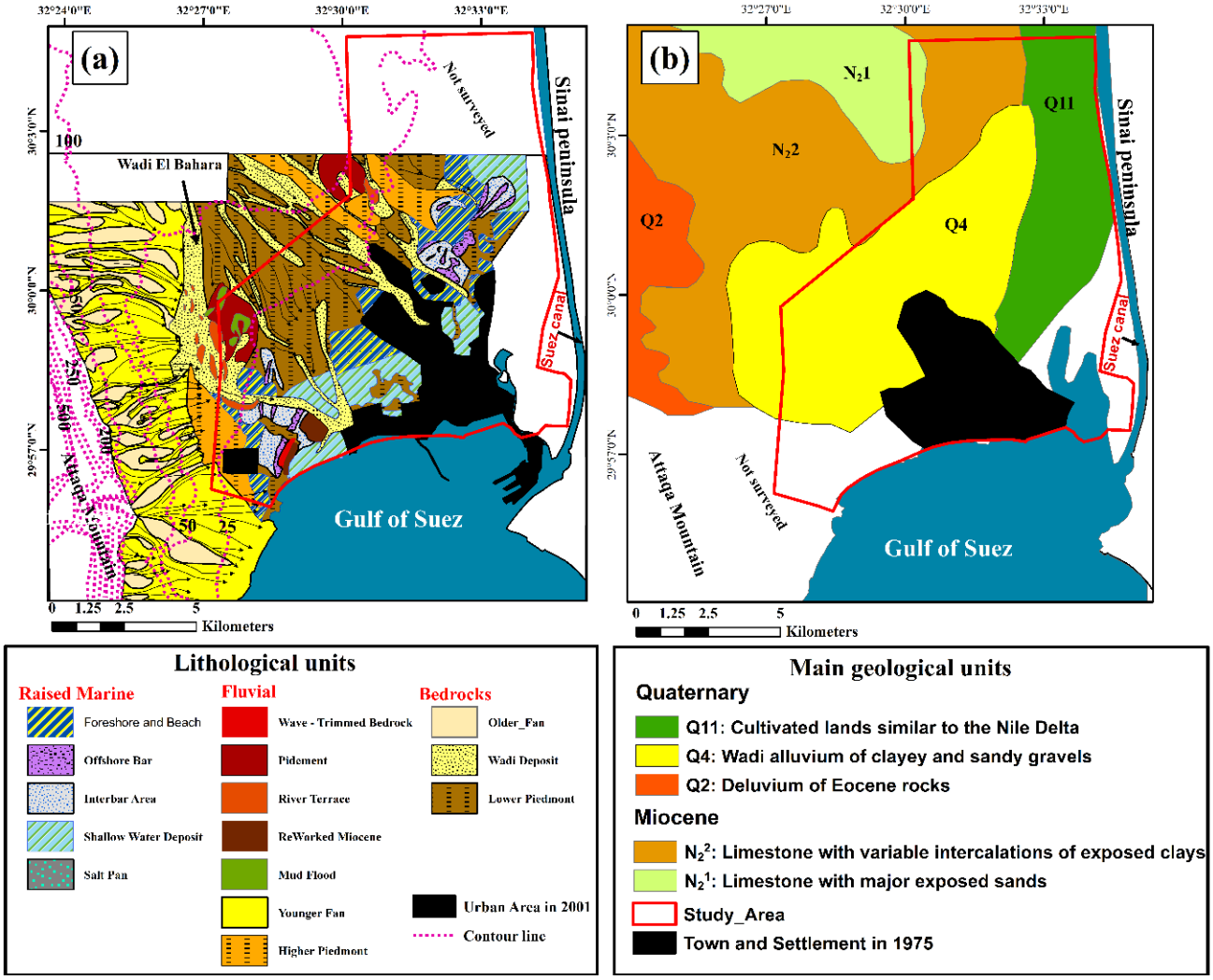

Fig. 2. Site characterization. (a) Geomorphological map showing the surface lithological units in a part of Suez city (modified after Jones, 2001); also shown is the surface elevation (pink dashed lines) extracted from a topographic map prepared by USA Army map services (AMS, 1956). (b) The distribution of main geological units in the northwestern part of the Gulf of Suez (modified after El Shazly et al., 1975). The location of the study area is shown as a red polygon.

2. Study area characteristics

The study area is located on the north-western part of the Gulf of Suez (Fig. 1c) and covers a total area of 131.3 km2. Suez is a growing industrial and commercial city regarding natural resources and activities. The Gulf of Suez, Suez Canal, and quarries (i.e., gravel, sand, limestone, and dolomite) are examples of environmental resources. Economic activities, such as the oil distillation industry, fertilizers, chemicals companies, and shipping services, are extensively existed in the southern part of the area under investigation. In terms of population, Suez is the fourth largest coastal city in Egypt with 0.76 million inhabitants (Hussein, 2018). Further, the average inhabited density of Suez Governorate is 68.3 Pop. /km2 and the percentage of inhabited to the total area is 100 % (Egyptian Survey Authority, 2012). Suez is divided into five main regions: El-Suez, El-Arbaeen, El-Ganayen, Feisal, and Attaqa (Fig. 1c). The distribution of population density varies over the five districts; the highly populated areas in decreasing order are El-Arbaeen, Feisal, and El-Ganayen districts (Ahmed, 2018).

Suez's climate is characterized by a moderate winter and a hot and long summer (15°C to 42°C), with an average humidity of 60% in winter and 45% in Summer (Egyptian Meteorological Authority, 1996). Rainfall is low and sparse with an annual average precipitation of 23.6 mm (Awadallah et al., 2017). Seasonal fluctuations in the mean sea level recorded high rates from November to April, with a daily tidal difference of about 121 cm along the southern coast of the investigated area (Eid et al., 1997).

Geomorphologically, the investigated area can be mainly classified from west to east into three topographical units (Fig. 2a): high terrain, alluvial fans, and low land. The high terrain is up-faulted limestone of Attaqa mountain (≈

850 m above sea level, a.s.l), located on the western part of the area under study. The low isthmus land is a coastal fringe of raised marine deposits, which are dissected by coarse sub-watersheds initiated from Attaqa mountain that form the mainstream of Wadi El-Bahhara (Jones, 2001). According to El Shazly et al. (1975), the isthmus stretch extends from the Gulf of Suez in the south to near the El-Ballah lagoon in the north. Suez districts were built on the isthmus stretch, which is covered by Quaternary deposits (El Shazly et al., 1975). These deposits are broadly spread over the study area as wadi alluvium of clayey and sandy gravels (Q4) and cultivated muddy lands (Q11) similar to the Nile Delta (Fig. 2b). The Hommath Formation of Middle Miocene bedrock, which is composed of limestone with variable intercalations of clays (N22) and sands/sandstone (N21), is observed in the northern part of the study area (Abdalla and Abdel Hady, 1966).

The hydrogeological regimes comprise: (1) the eastern part of Suez is crossed by the El-Suez freshwater canal (Fig. 1c), a branch of the El-Ismailia Canal, which is the sole source of drinking water and agriculture irrigation, and (2) four subsurface aquifers of high salinity water, including but not limited to, Quaternary, Miocene, Oligocene, and Eocene (El Said, 1962 and El Shazly, et al., 1975). The shallow Quaternary aquifer is composed of gravel, sandstone rocks, and clayey sand, which is recharged mainly from seepages of freshwater pipes and agricultural schemes (Jones, 2001).

3. Materials & methods

In this study, the systematic procedure adopted to evaluate the LULC changes was data collection, preprocessing steps, image classification, and post-classification analysis (Fig. 3), described in the subsequent sections.

3.1. Overview of Data collection

Four multispectral satellite scenes (path 176, row 39) were acquired from three Landsat (TM, ETM, OLI) sensors of the years 1986, 2000, 2013, and 2018 (Table. 1). They were freely downloaded from the USGS database (EarthExplorer, 2018) as Digital Number (DN) with a spatial resolution of 30 m for visible, near-infrared (NIR), and short infrared (SWIR) bands (Table. 1). The data acquired were cloud-free scenes (less than 0.1%) and in the same season (November-March) to reduce misclassification errors (Verpoorter et al., 2012). The geo-referenced ancillary data includes ground truth locations using Garmin (GPSMAP 78) device, Google Earth imagery, geological map, and aerial-based geomorphological map (1:25000), along with a population data from 1986 to 2018. All data were stored in a relational GIS-based database implemented in ArcGIS environments to use later for image classification, accuracy assessment, and interpretations. Table (1) describes the various datasets sources utilized in this work.

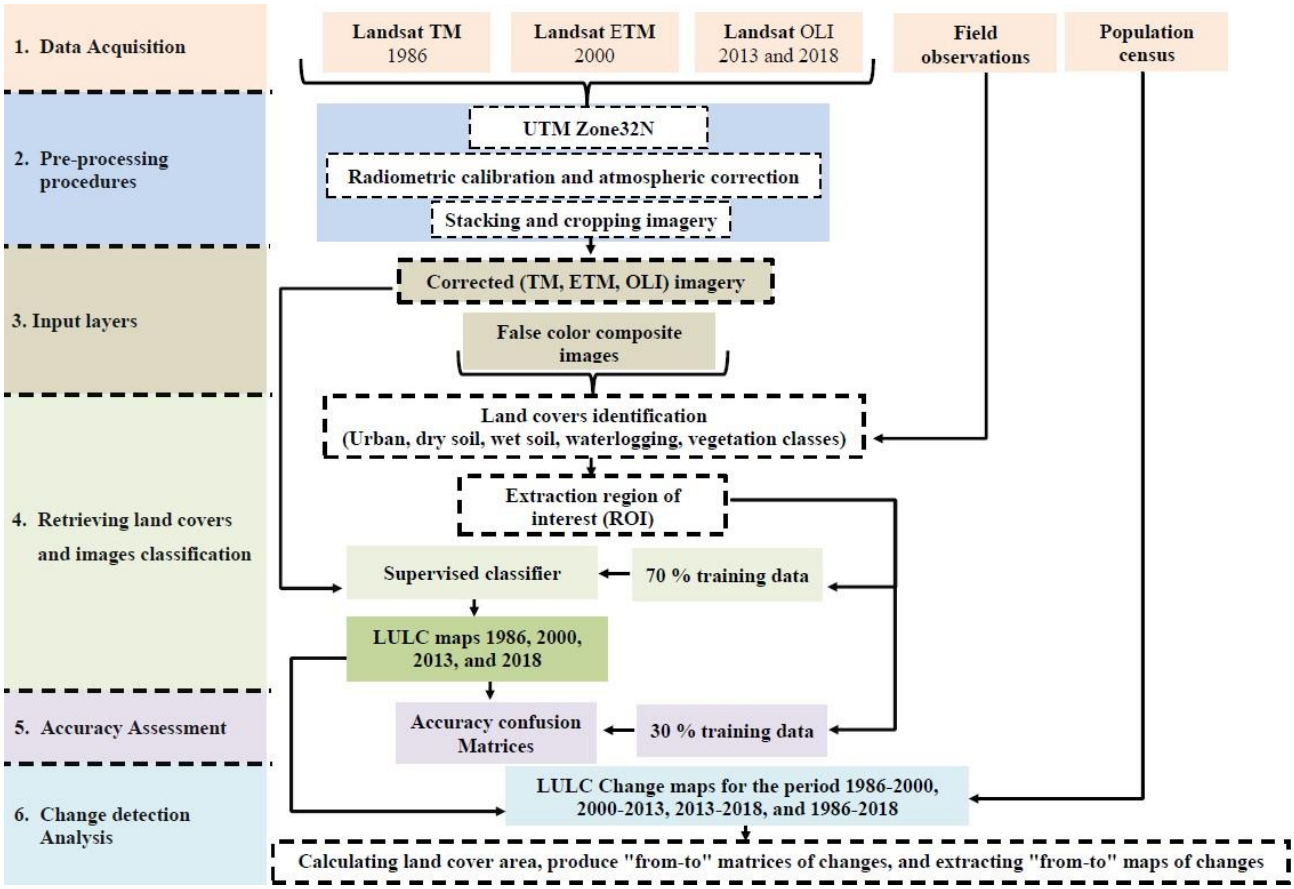

Fig. 3. Flow chart illustrating the methodology employed in this work.

Table. 1. List of datasets used in the study.

Data type	Datasets	Date	Specification	Source
Ancillary Data	Geological map	1975	The main geological units and the urban settlements boundary	El Shazly et al. (1975)
	Geomorphological map	2001	Understanding the nature of the surficial soil and site urban (built-up, roads, and industrial areas) pattern	Jones (2001)
	Land cover types	2018	LCs information for the LULC classification and assessment	Field survey and Google Earth pro
	Population Census	1986-2018	Suez population number for the years 1986, 2000, 2013, 2018	CAPMAS (2000) and Hussein (2018)
Remote sensing data*	Landsat TM	13/1/1986	Band 1- B (30m) Band 2- G (30m) Band 3- R (30m) Band 4- NIR (30m) Band 5- SWIR 1 (30m) Band 7- SWIR 2 (30m)	https://glovis.usgs.gov/app?fullscreen=1
	*****Landsat ETM+	11/11/2000		
	*****Landsat OLI	29/3/2013	Band 2- B (30m) Band 3- G (30m) Band 4- R (30m) Band 5- NIR (30m) Band 6- SWIR 1 (30m) Band 7- SWIR 2 (30m)	
		22/2/2018		

* Only non-thermal bands of Landsat (ETM and OLI) images (no panchromatic or thermal bands) were used during the analysis

3.2. Remotely Sensed Data Preprocessing

To prepare Landsat images for change detection, various preprocessing steps were applied, including geometric rectification, atmospheric correction, and data stacking and clipping. All scenes were co-registered to the Universal Transverse Mercator (UTM)) coordinate system, zone 36 North with a World Geodetic System (WGS) 1984 datum using the ArcMap (10.8) package established by ESRI (2020). After that, the radiometric normalization and atmospheric corrections were performed to make all images tonally balanced using the calibration tools and the fast line-of-sight atmospheric adjustment of spectral hypercubes (FLAASH) scheme in ENVI 5.1 package (Chavez, 1996; Perkins et al., 2005; Schroeder et al., 2006). Lastly, the six non-thermal corrected bands (1, 2, 3, 4, 5, and 7) of TM and ETM and (2, 3, 4, 5, 6, and 7) of OLI of each scene were stacked and cropped using the study area boundaries. To refine the visual perception of bands, false color composite (FCC) images of the optimal band combination were created and then enhanced using the Histogram equalization (Richards, 2012).

3.3. Retrieving and Classification of Land Use/Land Cover

The notion of the classification method is to assign pixels inherent in an image to various land cover classes (Campbell, 1987). Computer-based classifying of a remotely sensed image can be partitioned into supervised and unsupervised, and we used the former in this research. The maximum likelihood classifier (MLC) was performed to produce LULC maps. MLC, which is one of the most precise supervised classifiers (Lillesand and Kiefer, 1994; Liaqat et al., 2021), requires using an adequate number of training samples that represent distinct spectral signatures of land cover classes. Depending on the FCC images, which were gathered with old maps and Google Earth imagery, the regions of interest (ROIs) samples were visually determined using image interpretation keys (tone, shape, and association between land covers). Few field trips were conducted in 2018 (February to March) to survey and confirm the land cover types (Fig. 4). A random selection of 70 % from the ROIs inventory database was established to train the classification, while the remaining 30% was adopted as validation data. The four images of the years 1986, 2000, 2013, and 2018 were classified independently using related training classes for each date. Consequently, the area under study was categorized into 5 main classes: urban area, vegetation, dry bare soil, wet soil lands, and waterlogged areas.

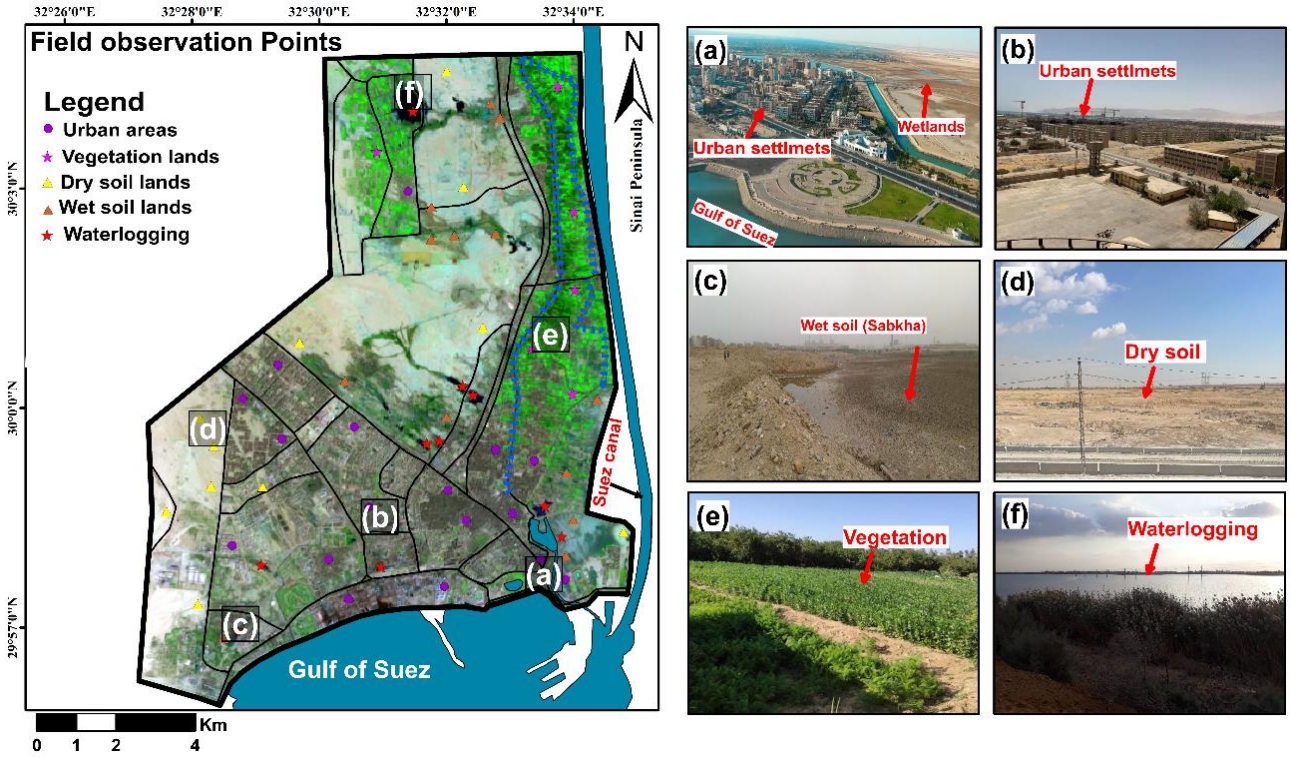

Fig. 4. Spatial distribution of field observation points with some collected photos of different LULC types (indicated on the image with white label) during fieldwork at Suez, Egypt: (a and b) urban areas comprise built-up and roads in the middle and southeastern parts of the study area, (c) Wet soil (Sabkha) lands near to the coastal area, (d) dry soil in the most western parts, (e) healthy vegetation land in El-Ganayen districts, and (f) waterlogging area near to Youssef El-Sebay

3.4. Post-classification analysis

Accuracy assessment is a widely employed method for evaluating the reality of the resulting LULC map against actual reference data using a confusion matrix (Campbell, 1996). The classification accuracies were performed separately for each LULC map (1986-2018) using the testing data. The classification of Landsat data was considered to be reliable if the value of overall accuracy (OA) is over 85% with no single class lower than 70% and Kappa coefficient value close to 1 (Lunetta and Lyon, 2004).

The post-classification comparison has proven to be a robust method for detecting land cover (pixel by pixel) change by comparing two independently classified images from different dates (Singh, 1989; Shalaby and Tateishi, 2007). The PCC method not only detects the spatial patterns of changes that have occurred but also attempts to quantify the nature of these changes “from-to” through comprehensive statistics (Jensen, 2005). Two successive LULC images for each period (i.e., 1986-2000, 2000-2013, and 2013-2018) were merged to create a new thematic map “from-to” and associated table of changes using the intersect tool in ArcMap.

4. Result and Discussion

4.1 LULC Maps and Validation

Retrieving types of land cover from multi-temporal images is an essential stage, with a special focus on the detection of urban areas, to understand the nature and patterns of urbanization and their potential influence on the study area. The optimal FCC composite images represent Landsat TM and ETM (7, 4, and 2 bands in RGB), and Landsat (7, 5, and 3 in RGB) OLI (Fig. 5). The urban areas can be identified by their distinctive geometry such as lines (roads) and rectangles (houses and industrial areas), which appear very clearly as dark brown tones in FCC images (Figs. 5 and 4a-b). The class of dry soil comprises fallow lands of Quaternary deposits and Miocene bedrock in the western parts (Figs. 2, 4d, and 5), which have strong reflectance pattern in all bands (Fig. 6). The vegetation class represents both agriculture and scanty plants that appear as dull-to bright-green colors (Fig. 4e and 5) with a high reflectance value in NIR (Fig. 6). The salty muddy and poorly drained soils were similar in spectral reflectance that appear in bluish brown tones in all FCC, and therefore, both were combined in one class "wet soil". (Fig. 4c and 5). The spectral reflectance patterns were deemed to be acceptable (Fig. 6a-d) as the confusion is minimal between the extracted land covers (Khan, et al. 2005; Gao and Liu, 2010).

Figure 7 shows the LULC classification of the study area for the years 1986, 2000, 2013, and 2018. Five LULC classes were created and symbolized into distinct colors to observe the features and analyze the direction of changes.

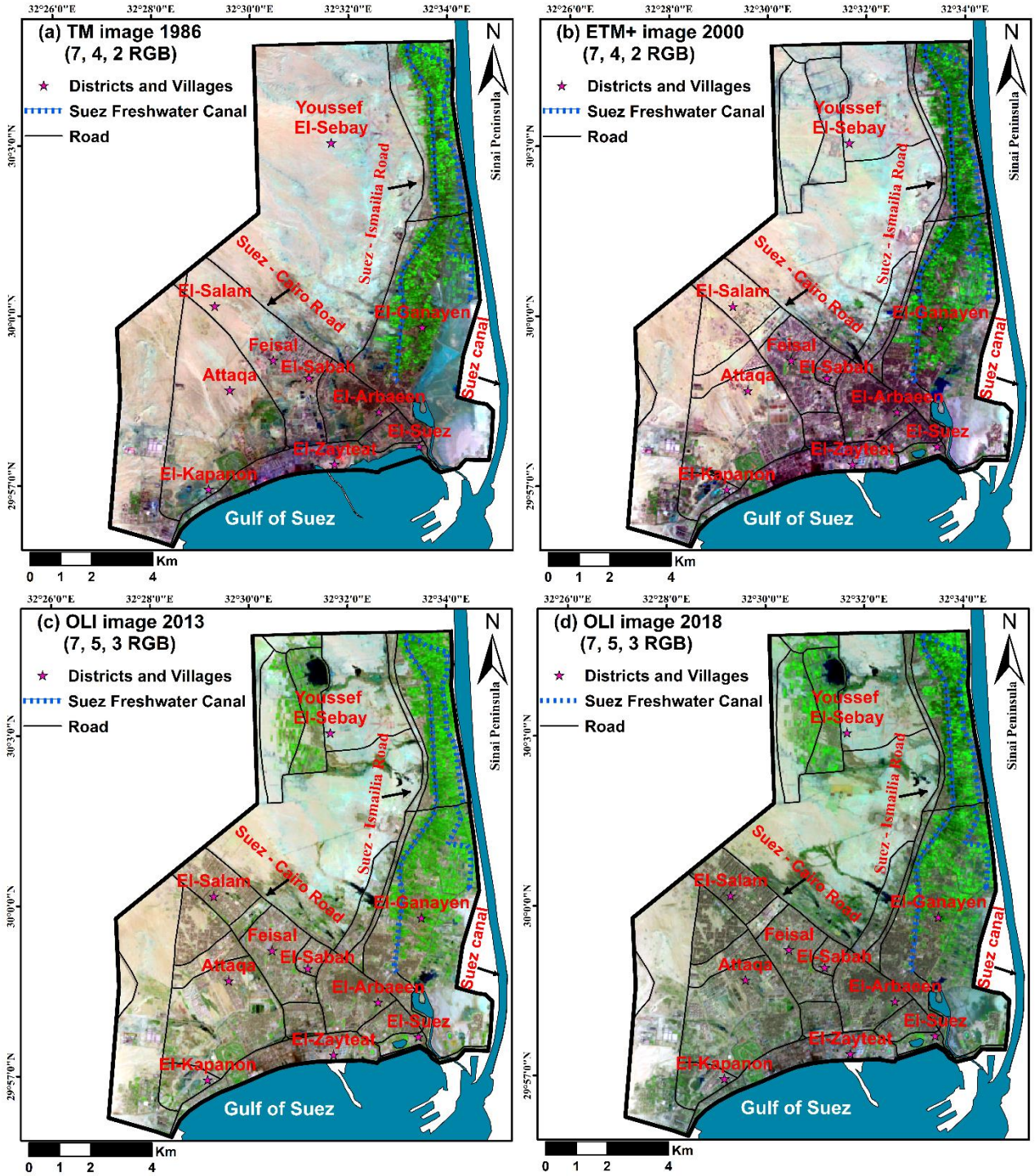

Fig. 5. Multi-temporal Landsat images of the selected date (1986 to 2018) represent the false-colour composite (FCC) after preprocessing step.

Before utilizing the classified maps, the accuracy was calculated by producing the error matrices for each year (Table 2). Respectively for 1986, 2000, 2013 and 2018 images, overall accuracies were 92.28 %, 92.45 % , 94.7 %, and 96.4 %, while the Kappa coefficient were 0.75, 0.8, 0.93, and 0.95, indicating the reliability of the classification. Moreover, all classes had producer's accuracy greater than 85%, while in terms of user's accuracy, all classes except the wet bare soil were over 90% for all dates.

4.2. Quantifying the land cover changes and driving forces

The classified maps showed dynamic change among the majority of land cover classes over the study period (Fig. 7a-d), which may reflect the potential impact of anthropogenic.

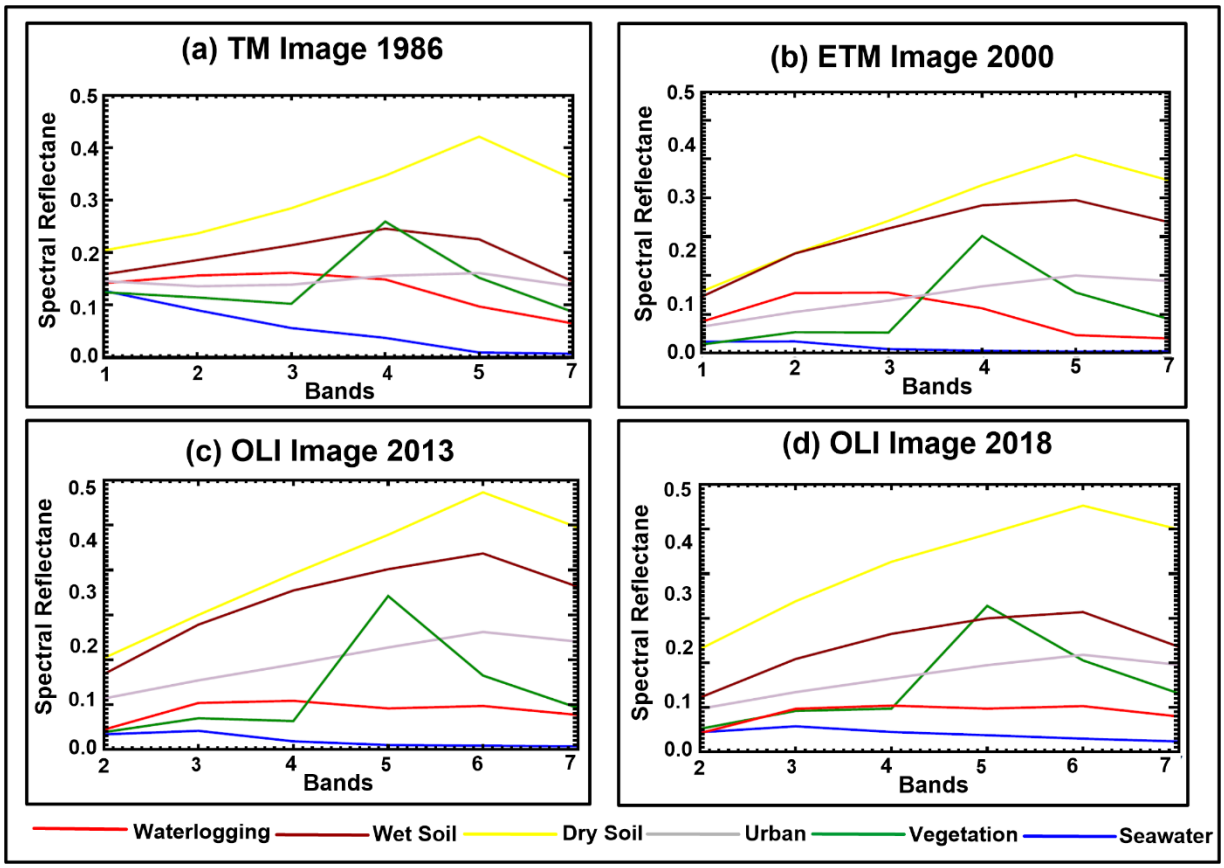

Fig. 6. Spectral response patterns curves for land cover classes (dry soil: yellow color, wet soil: brown color, urban: grey color, seawater: blue color, waterlogging: red color and vegetation: green color) of multi-temporal Landsat data, where the y-axis represents reflectance values for spectral bands on the x-axis (see Table (1) for the acronyms of bands (B1 to B7))

Table. 2. Accuracy assessments of the classified images of the years 1986, 2013, 2013 and 2018

Years	Classes	Reference data					Classified accuracy %	
		Dry soil	Urban	Vegetation	Waterlogging	Wet soil	Producer's accuracy	User's accuracy
2018	Dry Soil	70	0	0	0	0	100.0	100.0
	Urban	0	86	1	0	5	97.7	93.5
	Vegetation	0	0	59	0	2	98.3	96.7
	Waterlogging	0	1	0	33	0	97.1	97.1
	Wet Soil	0	1	0	1	47	87.0	95.9
	Overall accuracy (%)	96.4						
	Kappa coefficient	0.95						
2013	Dry Soil	70	0	0	0	0	100.00	100.00
	Urban	0	83	0	0	6	94.32	93.26
	Vegetation	0	0	58	1	2	96.67	95.08
	Waterlogging	0	1	2	33	0	97.06	91.67
	Wet Soil	0	4	0	0	46	85.19	92.00
	Total Accuracy	94.7						
	Kappa coefficient	0.93						

2000	Dry Soil	69	2	0	1	3	97.57	92.00
	Urban	0	73	3	1	2	95.59	92.41
	Vegetation	0	0	55	1	1	92.67	96.49
	Waterlogging	0	1	0	24	1	90.71	92.31
	Wet Soil	1	2	2	1	42	92.71	87.50
	Total Accuracy	92.45						
	Kappa coefficient	0.8						
1986	Dry Soil	69	2	0	1	3	98.57	92.00
	Urban	0	73	3	1	2	93.59	92.41
	Vegetation	0	0	55	1	1	91.67	96.49
	Waterlogging	0	1	0	24	1	85.71	92.31
	Wet Soil	1	2	2	1	42	85.71	87.50
	Total Accuracy	92.28						
	Kappa coefficient	0.75						

In this work, special emphasis is given to the dry soil, urban, and vegetation areas, which represent the highly dominant classes in the investigated area (Fig. 7e and Table 3). The results showed that from 1986 to 2018, a remarkable increase in urban, vegetation, wet soil, and waterlogging classes by 80.99%, 37.48%, 30.3%, and 4.77%, respectively, while the net area of dry bare soil declined by 47.33% (Table 4).

The spatial dynamics of LULC changes for the three periods of 1986–2000, 2000–2013, and 2013-2018 were displayed in figures 8, 9, and 10, respectively. Analysis results showed that drylands dominate a significant portion of the study area in 1986, representing 52.93% (70.19 Km^2). While it has decreased to 44.35% (58.83 Km^2) in 2000 (Fig. 7a-b and Table 3), with a net loss of 16.21% (or 11.38 km^2), see Table. 4. The population of the Suez increased from 328000 in 1986 to 450000 in 2000 (Central Agency for Public Mobilization and Statistics (CAPMAS), 2000). Consequently, the corresponding pixels of dry soil, wet soil, waterlogging, and vegetation areas class (7.81 km^2, 5.32 Km^2, 1.62 Km^2 and 2.21 Km^2) were transformed into urban class between 1986 and 2000 (Table 5). Most notably, the changes regarding wet soil, waterlogging, and vegetation areas have occurred within the old districts (Feisal, El-Sabah, Al-Arbaeen and south Al-Ganayen), as seen in Fig. 8. Consequently, the urban class has increased significantly from 28.04 Km^2 (21.14%) in 1986 to 39.75 Km^2 (29.98%) of the total area in 2000, with a total addition of 41.76% (Tables 3 and 4). Moreover, the wet soil and waterlogging areas (i.e., wetlands) decreased by 36.71% (2.84 Km^2) between 1986 and 2000, of which 1.25 and 1.37 Km^2 were converted into vegetation lands, respectively (Tables 4 and 5). This can be observed through the farmlands reclamation projects over the wetlands in the south-eastern part (Fig. 8). Results showed that infill growth (Kamh et al., 2012) and urban fringe developments (Heimlich and Anderson, 2001) were the dominant models during the first period. Where the urban growth has mainly occurred close to the main facilities (i.e., Suez freshwater Canal, drains, and roads) in the old city.

In the subsequent periods of 2000-2013 and 2013-2018, the urban development also perceived an increase in the rate compared to the period of 1986-2000.

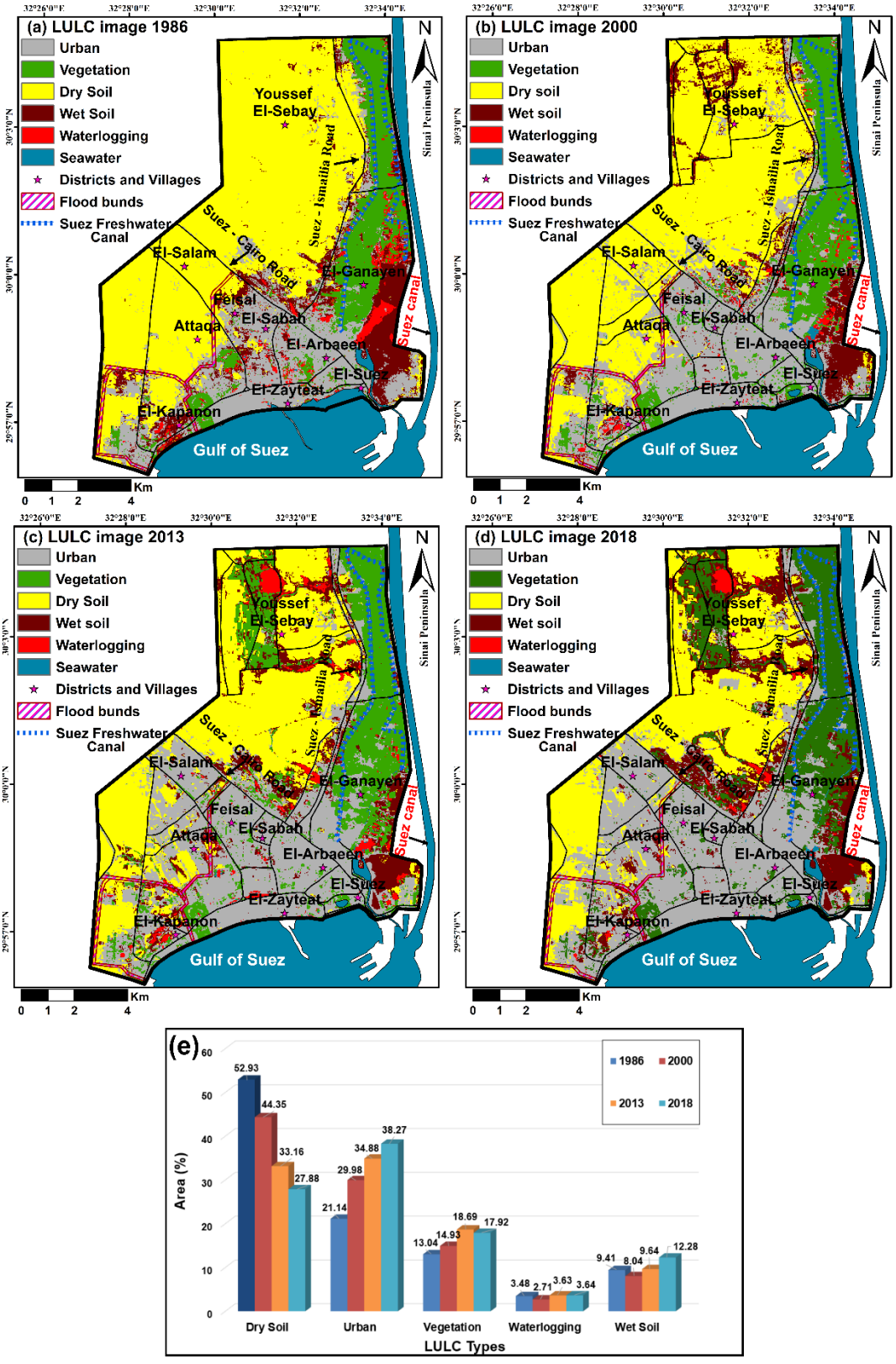

Fig. 7. Land use/land cover (LULC) maps in the study ((**a**) 1986, (**b**) 2002, (**c**) 2013 and (**d**) 2018); (**e**) The percentage of the LULC areas derived from the classified maps over 32 years.

Table. 3. Areal extent and percentages of the LULC classes of the years 1986, 2000, 2013, and 2018

	1986		2000		2013		2018	
Classes	Km^2	%	Km^2	%	Km^2	%	Km^2	%
Dry Soil	70.19	52.93	58.83	44.35	44	33.16	36.97	27.88
Urban	28.04	21.14	39.75	29.98	46.26	34.88	52.06	38.27
Vegetation	17.29	13.04	19.8	14.93	24.78	18.69	23.77	17.92
Waterlogging	4.61	3.48	3.59	2.71	4.81	3.63	4.83	3.64
Wet Soil	12.48	9.41	10.66	8.04	12.79	9.64	16.29	12.28

Table. 4. The area and amount of change in different LULC categories in the study area between the different dates. Percentages were computed relative to the area of the older date and the negative sign (-) reveals a decline in the land cover class

	Difference 1986-2000		Difference 2000-2013		Difference 2013-2018		Difference 1986-2018	
Classes	Km^2	%	Km^2	%	Km^2	%	Km^2	%
Dry Soil	-11.38	-16.21	-14.84	-25.23	-7	-15.92	-33.22	-47.33
Urban	11.71	41.76	6.51	16.38	4.49	9.71	22.71	80.99
Vegetation	2.51	14.52	4.98	25.15	-1.01	-4.08	6.48	37.48
Waterlogging	-1.02	-22.13	1.22	33.98	0.02	0.42	0.22	4.77
Wet Soil	-1.82	-14.58	2.13	19.98	3.5	27.37	3.81	30.53

Table. 5. Showing matrices of change detection calculations of LULC classes between each pair of classified maps from 1986 to 2018

	Land Class	2000 (Km^2)				
		Dry Soil	Urban	Vegetation	Waterlogging	Wet Soil
1986 (Km^2)	Dry Soil	**57.24**	7.81	0.35	0.29	4.50
	Urban	0.95	**22.79**	2.40	0.60	1.30
	Vegetation	0.05	2.21	**14.42**	0.57	0.04
	Waterlogging	0.04	1.62	1.37	**1.27**	0.31
	Wet Soil	0.55	5.32	1.25	0.85	**4.51**
		2013 (Km^2)				
2000 (Km^2)	Dry Soil	**39.83**	9.07	4.09	1.07	4.78
	Urban	2.26	**31.56**	2.32	0.97	2.65
	Vegetation	0.03	3.27	**16.03**	0.32	0.15
	Waterlogging	0.05	0.68	1.07	**1.49**	0.29
	Wet Soil	1.83	1.68	1.27	0.96	**4.92**
		2018 (Km^2)				
2013 (Km^2)	Dry Soil	**35.20**	4.16	0.92	0.05	3.90
	Urban	0.89	**41.43**	1.54	0.19	2.25
	Vegetation	0.19	3.12	**18.72**	1.19	1.56
	Waterlogging	0.03	0.99	0.49	**2.19**	0.14
	Wet Soil	0.67	2.37	1.11	1.20	**8.45**

Values in bold correspond for class unchanged value

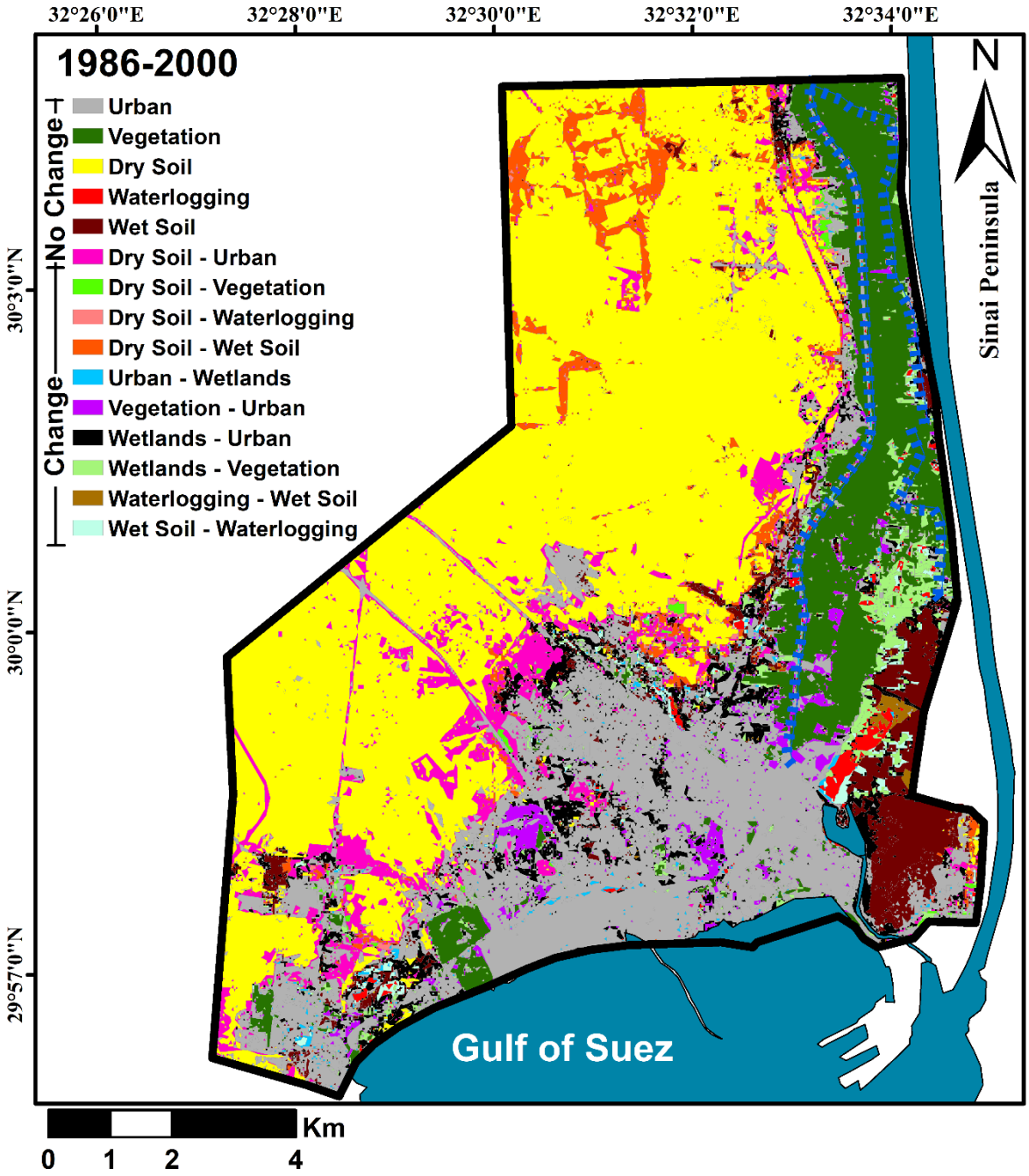

Fig. 8. The spatial distribution of LULC changes in the study area from 1986 to 2000.

The Suez population increased from around 510,000 in 2006 to 599.320 in 2013, and then significantly raised to 761,000 in 2017 (Hussein, 2018). The Attaqa mountain, Gulf of Suez, and Suez Canal represent natural geomorphological constraints for the urban expansion in the western, southern, and eastern directions, respectively. For a more rationally solution, the urban projects have expanded in a linear pattern toward the northwestern and northern directions during 2000-2013 (Fig. 9) and 2013-2018 (Fig. 10). Therefore, the dry soil has decreased by 14.84 km^2 (25.23%) and 7 km^2 (15.92%), of which 9.07 km^2 and 4.16 km^2 were converted to urban class during 2000-2013 and 2013-2018, respectively (Tables 4 and 5). Accordingly, the area of the urban class increased by 16.38% and 9.71% in the periods of 2000-2013 and 2013-2018, respectively (Table 4). Similarly, the progress of agriculture projects in the northern part accelerated the growth of vegetation areas from 19.8 Km^2 in 2000 to around 24.78 Km^2 in 2013, an increase of about 25.15%, then decreased by 4.08% (1.01 Km^2) in 2018 (Tables 3 and 4). As mentioned early, there is also a noticeable decrease in the cultivated lands toward build-up (i.e., conversions from vegetation to urban class) between 2000 and 2018 (Figs. 9-10).

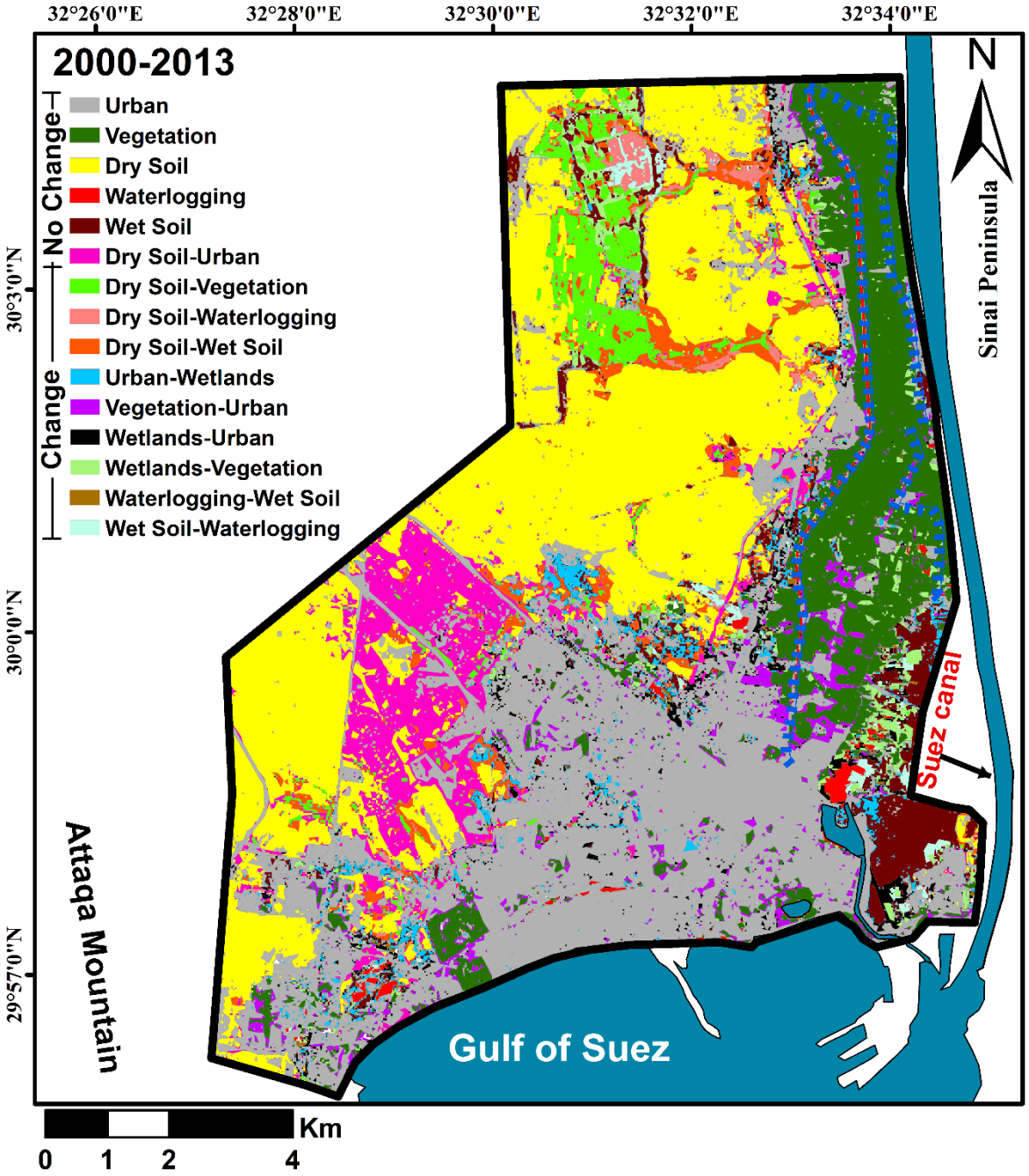

Fig. 9. The spatial distribution of LULC changes in the area of study from 2000 to 2013.

According to El-Kholei (2004), various interrelated urban problems observed in Suez, i.e., uneven population distribution and growing informal areas, are consequences of the increasing rural-urban migration from upper Egypt to Suez city, and that was observed in our study. These observations could be related to some illegal urban sprawl over the agricultural lands in the southern portion of the El-Ganayen district, which reflects the dominance of the inner growth model from 2013 to 2018. Therefore, the urban cover represents the largest class in 2013 and 2018, occupying 46.26 km^2 (34.88%) and 52.06 km^2 (38.87%) of the study area, respectively (Table 3).

In terms of environmental changes, the cultivation process changed the soil condition in the northern part (Youssef El-Sebay), started with wetting drylands in 2000 (Fig. 8), which developed over time to waterlogging class in 2013 (Fig. 9) and hence limited the usage of these areas in 2018 (Fig. 4.10). As a result, the wet soil areas regained a total of 2.13 Km^2 (19.98%) and 3.5 Km^2 (27.37%) in the periods of 2000-2013 and 2013-2018, respectively (Table 4). This agrees with the increase in the waterlogging area during the period 2000-2013 by 1.22 Km2 (33.98%), while minor changes during 2013-2018. This seems to be the result of intensive agricultural practices in the Youssef El-Sebay area over the study

period. Sadly, these wetlands imply shallow groundwater levels with the high salinity in Youssef El-Sebay area (El Omla and Aboulela, 2012; Youssef et al., 2021), which are problematic sites for urban sustainability projects (Andriamamonjisoa and Hubert-Ferrari, 2019). On the other hand, the occurrence of permanent wetlands was observed near the south-eastern and south-western coastal borders of Suez city from 1986 to 2018 (Figs. 8-10).

Generally, the temporal dynamic of the Suez coastal area reflects the potential impact of rapid urbanization on the nature and rate of change in land covers. The current findings are in line with previous research in different coastal areas (i.e., Kamh et al., 2012; El-Zeiny and Effat, 2017, Ahmed, 2018; Zaghloul et al., 2020; Acharki et al., 2022). Similar findings were also noticed in the northern area of the Suez Canal, where human activities – especially rapid urbanization and land reclamation – have transformed the drylands into urban, agricultural, and salt-affected lands (Arnous and green, 2015; El Zeniy et al., 2022). It seems that the government agencies could not deal with the emerging geo-environmental problems that followed the coastal urbanization in Suez (Egypt). This study will provide the decision-makers with the current and updated information on the coastal urbanization and associated land degradation in Suez in a remote sensing and GIS framework.

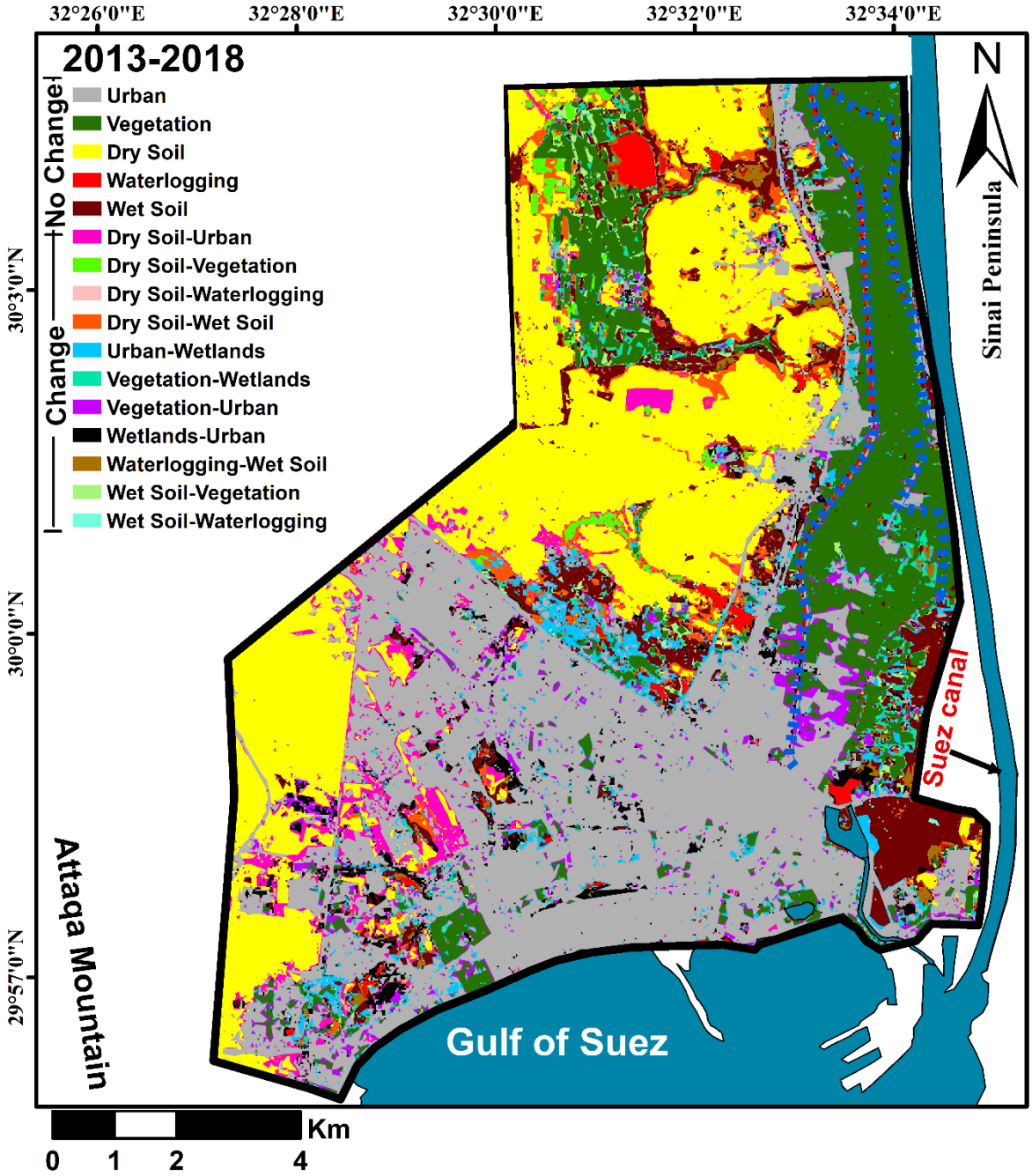

Fig. 10. The spatial distribution of LULC changes in the area under investigation from 2013 to 2018.

5. Conclusion

Rapid monitoring of LULC change, especially in coastal cities, was indispensable for sustainable land use and sustainable agricultural development. This study explained a methodology that attempts to detect urban land cover changes in Suez (Egypt) using the retrieved data of Landsat spanning three decades (1986-2018). The findings of this study can be summarized as follows:

1. Five land cover classes were identified in the investigated area, based on visual analysis of FCC images, to acquire classified images of the years 1986, 2000, 2013, and 2018.
2. Post-classification analysis of the classified images showed that two developmental schemes, specifically urbanization and land reclamation, have increased the urban areas at the expense of dry soil area during the study period. The urban area increased by 80.99% between 1986 and 2018, occupying 38.27% (52.06 Km^2) of the study area in 2018. Similarly, the vegetation areas expanded from 17.29 Km^2 in 1986 to 23.77 Km^2 in 2018, an increase of 37.48 %. Accordingly, dry soil decreased from 70.19 Km^2 (52.93%) in 1986 to 36.97 Km^2 (27.88%) in 2018, with a total loss of 47.33%.
3. Unfortunately, haphazard urban expansion was observed over the agricultural lands in the southern part of the El-Ganayen district in all periods of 1986-2000, 2000-2013, and 2013-2018. Moreover, unmanaged human practices have extremely deteriorated land covers in the northern regions, affecting agricultural sustainability. As a result, an increase in the waterlogging and wet soil classes was observed during the investigated period (1986-2018).
4. The integration of change detection analysis and demographic data showed that population growth is believed to be the main factor driving the urban expansion in Suez. Additionally, the natural geographic determinants constrained the spatial pattern of urban expansion, where infill, linear growth, and urban fringe development are the dominant models.

Overall, this work has significant importance for sustainable development strategies in Egypt under rapid urbanization. The migration of rural citizens to coastal cities, which is considered one of the most contemporary issues, is changing landscape patterns and thus, affecting land sustainability, vegetation diversity, and environmental security. Understanding the reasons and consequences of rapid LULC changes will assist the governmental agencies in future planning and mitigation strategies. The present work indicates that the integration of multi-temporal remotely sensed imagery and ancillary data in the GIS environment was extremely effective in detecting LULC changes and this, in turn, provided a powerful approach for updating land cover change information. Moreover, it can be employed as a preliminary geographical investigation to appraise the potential environmental hazards after urbanization. Present findings could be considered a milestone in the road map of urban planners for more rational land use management and appropriate planning in Suez.

Acknowledgments

The authors would like to thank the USGS for providing the Landsat datasets. Thanks are due to the Cultural Affairs and Missions Sector, Ministry of Higher Education, Egypt for the Channel Mission of Youssef Y.M., to the University of Tsukuba as a visiting PhD foreign research fellow.

References

Abd El-Kawy, O.R., Rød, J.K., Ismail, H.A., Suliman, A.S. (2011). Land use and land cover change detection in the western Nile delta of Egypt using remote sensing data. Applied Geography. 31(2), 483-494.

Abdalla, A.M., Abdel Hady, F.M. (1966). Geology of Sadat Area, Gulf of Suez. J. Geol. UAR. 10, 1pp.

Abu Salem H.A, Gemail Kh.S., Nosair A. (2021). A multidisciplinary approach for delineating wastewater flow paths in shallow groundwater aquifers: A case study in the southeastern part of the Nile Delta, Egypt, Journal of Contaminant Hydrology. https://doi.org/10.1016/j.jconhyd.2020.103701.

Abu Salem, H., Abu Khatita, A., Abdeen, M.M., Mohamed, E., El Kammar, A.M. (2017). Geo-environmental evaluation of Wadi El Raiyan Lakes, Egypt, using remote sensing and trace element techniques. Arabian J. Geosci. https://doi.org/10.1007/s12517-017-2991-3. AJGS-D-16-01723.2.

Acharki, S., El Qorchi, F., Arjdal, Y., Amharref, M., Bernoussi, A.S., Ben Aissa, H. (2022). Soil Erosion Assessment in Northwestern Morocco. Remote Sensing Appl. Soc. Environ. 25, 100663. doi:10.1016/j.rsase.2021.100663.

Ahmed, S. (2018). Assessment of urban heat islands and impact of climate change on socioeconomic over Suez Governorate using remote sensing and GIS techniques. The Egyptian Journal of Remote Sensing and Space Science, 21(1), 15–25.

Alberti, M., Weeks, R., Coe, S. (2004). Urban land cover change analysis in central Puget sound. Photogrammetric Engineering and Remote Sensing, 70, pp. 1043–1052.

Andriamamonjisoa, S.N., Hubert-Ferrari, T.O. (2019). Combining geology, geomorphology and geotechnical data for a safer urban extension: application to the antananarivo capital City (Madagascar). J Afr Earth Sc. 151,417–437.

Arnous. M., Green, D. (2015). Monitoring and assessing water-logged and salt-affected areas in the Eastern Nile Delta region, Egypt, using remotely sensed multi-temporal data and GIS. J Coast Conserv. 19, 369–391.

Awadallah, A.G., Magdy, M., Helmy, E., Rashed, E. (2017). Assessment of rainfall intensity equations enlisted in the Egyptian code for designing potable water and sewage networks. Advances in Meteorology. 2, 1–10.

Balk, D., Montgomermy M.R., McGranahanm, G., Kim, D., Mara, V., Todd, M., et al. (2009). Mapping urban settlements and the risks of climate change in Africa, Asia and South America. In: Guzmán JM, Martine G, McGranahan G, Schensul D and Tacoli C, editors. Population Dynamics and Climate Change. New York, London: United Nations Population Fund (UNFPA), International Institute for Environment and Development (IIED). 80–103.

Campbell, J.B. (1996). Introduction to Remote Sensing. 2nd Edition, Taylor and Francis, London: 621.

Campbell. J.B. (1987). Introduction into remote sensing. The Guildford Press, New York.

Central Agency for Public Mobilization and Statistics (CAPMAS), (2000). The Statistical Year Book, 1993-1999, June 2000.

Chavez, P.S. (1996). Image-based atmospheric correction-revisited and improved. Photogrammetric Engineering and Remote Sensing, 62, 1025–1036.

EarthExplorer. (2018). Retrieved from *http://earthexplorer.usgs.gov/*. Accessed 4 March 2018.

Eid, F.M., Sharaf El-Din, S.H., Alam El-Din, K.A. (1997). Sea-level Variation along the Suez Canal. Estuarine, Coastal and Shelf Science. 44, 613–619.

El Omla, M.M., Aboulela, H.A. (2012). Environmental and Mineralogical Studies of the Sabkhas Soil at Ismailia—Suez Roadbed, Southern of Suez Canal District, Egypt. Open Journal of Geology. 2, 165-181.

El Shazly, E.M., Abd El Hady, M.A., El Shazly, M.M., El Kassas, I.A., El Ghawaby, M.A., Salman, A.B., Morsi, M.A. (1975). Geology and groundwater potential studies of El Ismailia master plan study area. Remote Sensing Research Project, Academy of Scientific Res. and Techno, Cairo, Egypt.

Elagouz, M.H., Abou-Shleel, S.M., Belal, A., El-Mohandes, M.A.O. (2020). Detection of land use/cover change in Egyptian Nile Delta using remote sensing, Egypt. J. Remote Sens. Space. Sci. 23, 57–62.

El-Kholei A.O. (2004). The Environmental Profile of the Governorate of Suez. Technical Report https ://doi.org/10.13140/RG.2.1.3772.8406

Egyptian Meteorological Authority. (1996). Climate Atlas of Egypt. Ministry of Transportation and Communication. http:// ema. gov. eg/

Elmahdy, S.I., Mohamed, M.M. (2016). Land use/land cover change impact on groundwater quantity and quality: a case study of Ajman Emirate, the United Arab Emirates, using remote sensing and GIS Arabian. J. Geosci. 9, 722.

El-Zeiny, A., Effat, H., Mansour, K., Shahin, A., Elwan, K. (2022). Geo-environmental monitoring of coastal and land resources of Port Said Governorate, Egypt, Egyptian. J. of Remote Sensing and Space Sciences. 25(1), 157-172. *https://doi.org/10.1016/j.ejrs.2022.01.009*.

El-Zeiny, A., El-Hefni, A., Sowilem, M. (2017). Geospatial technique for environmental modeling of breeding habitats at Suez Canal Zone, Egypt, The Egyptian. J. of Remote Sensing and Space Sciences. 2, 283–293.

Engelhardt, H., Schulz, F., Büyükkeçeci, Z. (2018). Demographic and human development in the Middle East and North Africa. Bamberg: University of Bamberg Press. https:// doi.org/10.20378/irbo-50993

Gao, J., Liu, Y. (2010). Determination of land degradation causes in Tongyu County, Northeast China via land cover change detection. Int J Appl Earth Obs Geoinf. 12, 9-16

Heimlich, R.E., Anderson, W.D. (2001). Development at the Urban Fringe and Beyond: Impacts on Agriculture and Rural Land, ERS Agricultural Economic Report No. 803 (Washington, DC: ERS, US Department of Agriculture). 88 p.

Hegazy, I.R. (2021). Towards sustainable urbanization of coastal cities: The case of Al-Arish City, Egypt. Ain Shams Eng. J. 12,2275–2284.

Hussein, A.S. (2018). Egypt's Demographic Opportunity Preliminary Assessment based on 2017. Census. UNFPA Egypt Country Office. CAPMAS and Faculty of Economics and Political Science. 24 p.

Jensen, J.R.E. (2004). Introductory Digital Image Processing: A remote sensing perspective 3rd edn. Prentice Hall, Upper Saddle River

Jiang, D., Huang, Y., Zhuang, D., Zhu, Y., Xu, X., Ren, H. (2012). A simple semi-automatic approach for land cover classification from multispectral remote sensing imagery. PloS One 7, e45889.

Jones, D.K.C. (2001). Ground conditions and hazards: Suez City development, Egypt. Geological Society, London, Engineering Geology Special Publications. 18, 159–169.

Kamh, S., Ashmawy, M., Kilias, A., Christaras, B. (2012). Evaluating urban land cover change in the Hurghada area, Egypt, by using GIS and remote sensing. International Journal of Remote Sensing. 33(1), 41–68.

Karlsson, C.S., Kalantari, Z., Mörtberg, U., Olofsson, B., Lyon, S.W. (2017). Natural Hazard Susceptibility Assessment for Road Planning Using Spatial Multi-Criteria Analysis. Environ. Manag. 60, 823–851.

Khan, N.M., Rastoskuev, V.V., Sato, Y., Shiozawa, S. (2005). Assessment of hydrosaline land degradation by using a simple approach of remote sensing indicators. Agric Water Manag. 77, 96–109.

Liaqat, M.U., Mohamed, M.M., Chowdhury, R., Elmahdy, S.I., Khan, Q., Ansari, R. (2021). Impact of Land Use/Land Cover Changes on Ground Water Resources in Al Ain Region of the United Arab Emirates Using Remote Sensing and GIS Techniques. Groundwater for Sustainable Development, 100587.

Lillesand, T.M., Kiefer, R.W. (2000). Remote sensing and image interpretation. Wiley, New York.

Lu, D., Mausel, P., Brondizio, E., Moran, E. (2004). Change detection techniques. International Journal of Remote Sensing. 25(12), 2365-2407.

Lunetta, R.S., Lyon, J.G., (Eds.) (2004). Remote sensing and GIS accuracy assessment. CRC press

McMichael, C., Dasgupta, S., Ayeb-Karlsson, S., Kelman, I. (2020). A review of estimating population exposure to sea-level rise and the relevance for migration. Environ Res Lett. 15(12),123005. https://doi.org/10.1088/1748-9326/abb398

Moufaddal, W.M. (2005). Use of satellite imagery as environmental impact assessment tool: a case study from the new Egyptian Red Sea coastal zone. Environmental Monitoring & Assessment. 107, 427–452.

Perkins, T., Adler-Golden, S., Matthew, M., et al. (2005). Retrieval of atmospheric properties from hyper and multispectral imagery with the FLAASH atmospheric correction algorithm. In Remote sensing of clouds and the atmosphere X, SPIE. 5979, 59790E-59791–59790E-59711.

Richards, J.A. (2013). Remote Sensing Digital Image Analysis. Springer, Berlin, Heidelberg. https://doi.org/10.1007/978-3-642-30062-2

Said, R. (1962). The Geology of Egypt. Amsterdam: Elsevier.

Schroeder, T.A., Cohen, W.B., Song, C., Canty, M.J., Yang, Z. (2006). Radiometric correction of multi-temporal Landsat data for characterization of early successional forest patterns in western Oregon. Remote Sens Environ. 103, 16-26.

Shalaby, A., Tateishi, R. (2007). Remote sensing and GIS for mapping and monitoring land cover and land-use changes in the Northwestern coastal zone of Egypt. Applied Geography. 27(1), 28-41.

Singh, A. (1989). Digital change detection techniques using remotely-sensed data. International Journal of Remote Sensing. 10(6), 989-1003.

The Egyptian General Survey Authority (2012). www.esa.gov.eg.

United Nations, Department of Economic and Social Affairs, Population Division (UNDESA/PD). (2019). World Urbanization Prospects 2018: Highlights (ST/ESA/SER.A/421).

USA Army map services (AMS). (1956). Topographic map of north Africa, Egypt. The PCL Map Collection, University of Texas at Austin. Sheets NH 36 - 6 and 10, series P502. Access at http://,aps.lib.utexas.edu/maps/ams/north_africa/

Verpoorter, C., Kutser, T., Tranvik, L. (2012). Automated mapping of water bodies using Landsat multispectral data. Limnology and Oceanography-Methods. 10, 1037–1050.

Youssef, Y.M., Gemail, K.S., Sugita, M., AlBarqawy, M., Teama, M.A., Koch, M., Saada, S.A. (2021). Natural and Anthropogenic Coastal Environmental Hazards: An Integrated Remote Sensing, GIS, and Geophysical-based Approach. Surv Geophys 42, 1109–1141. *https://doi.org/10.1007/s10712-021-09660-6*

Youssef, Y.M., Sugita, M., Gemail, K.S., Saada, S.A., Teama, M.A., AlBarqawy, M. (2020). An integrated GIS and Geophysical-based approach for geohazards risk assessment in coastal region: a Case study in Suez city, Egypt. Earth and Space Science Open Archive. p11, https://doi.org/10.1002/essoar.10506623.1

Zaghloul, E.A., Abdeen, M.M., Elbeih, S.F., Soliman, M.A. (2020). Waterlogging problems in Egypt's Deserts: Case study Abu Mena archaeological site using geospatial techniques, The Egyptian Journal of Remote Sensing and Space Sciences. https://doi.org/10.1016/j.ejrs.2020.06.003.